Control of Hysteretic Systems Through Inverse Compensation

RAM V. IYER and XIAOBO TAN

ALGORITHMS, ADAPTATION, AND EMBEDDED IMPLEMENTATION

DENNIS S. BERNSTEIN

In an 1881 study of ferromagnetism [37], James A. Ewing coined the term *hysteresis*, which means "to lag behind" in Greek. In Figure 1, which is reproduced from [1], the horizontal axis is the magnitude of the average magnetic field H in a soft-iron ring, while the vertical axis is the magnitude of the average magnetic flux density B. The plot was obtained by varying the magnetic field in a quasi-static manner and recording the average magnetic flux density. The following observations can be made from this example:

1) *Causality:* The output B depends on past and current values of the input H only.
2) *Monotonicity:* The output B increases and decreases with a corresponding change in the input H.
3) *Presence of a major loop:* The set of points in the (H, B) plane that can be reached lie between two curves that together form the major loop. The increasing part of this loop is obtained by first decreasing the magnetic field H to a large negative value $-H_{\max}$ for which the magnetic flux density saturates at $-B_{\max}$, and then increasing it to $H_{\max}$.
4) *Minor loop closure:* Suppose that the input H and output B at some instant are such that (H, B) is on the major loop. If the input is changed to a value $\tilde{H}$ and then changed back to H, then the output changes its value to $\tilde{B}$ and back to B. In other words, $(H, B) \to (\tilde{H}, \tilde{B}) \to (H, B)$.
5) *Energy Dissipation:* It can be shown that the energy needed from a power source to complete a loop, say between (H_1, B_1) and (H_2, B_2), is proportional to the area enclosed by the closed loop.
6) *Order Preservation:* The paths for increasing inputs in the (H, B) plane are nonintersecting, as are the paths for decreasing inputs.

Digital Object Identifier 10.1109/MCS.2008.930924

1066-033X/09/$25.00©2009IEEE

This article concerns control of systems with hysteresis composed of a hysteresis operator in a series connection with a linear system.

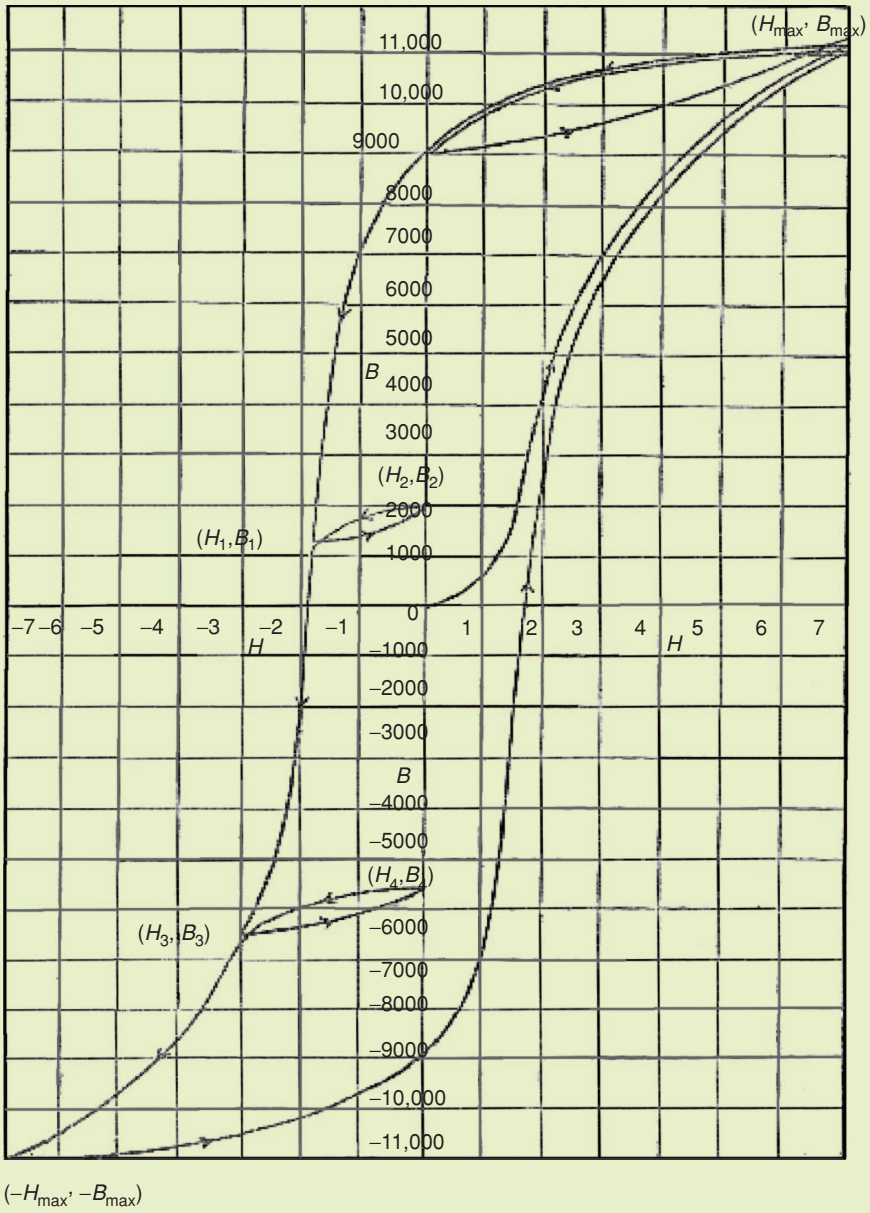

FIGURE 1 Experimental curves for a soft-iron ring [1]. The magnetic field is varied in a quasi-static manner, and the average magnetic flux density in the ring is recorded. A major loop in the (H, B)-plane is obtained when H is changed from a large negative value $-H_{max}$ to a large positive value H_{max} and vice versa. Suppose that the input is decreased from H_{max} to H_1 and then increased to a value H_2 that is less than H_{max}. When the input is decreased again to H_1, then the corresponding value of the flux density is B_1. In other words, the minor-loop inside the major loop closes on itself. From (H_1, B_1), when the input is reduced to H_3, increased to $H_4 < H_{max}$, and then reduced to H_3 again, the same phenomenon is observed.

Although these observations form the phenomenology of ferromagnetic hysteresis, they do not define hysteresis. Our next objective is to provide a precise mathematical definition of the hysteresis phenomenon as an operator mapping a function of time to another function of time. The physical causes of hysteresis are the presence of multiple metastable states of a thermodynamic free energy functional and energy dissipation. In the micromagnetic theory of ferromagnetism, crystalline symmetry results in multiple minima for the thermodynamic free energy giving rise to multiple metastable states. When an external magnetic field is applied to a ferromagnet, each individual magnetic moment precesses about the direction of the effective magnetic field and settles asymptotically in that direction [2], [3]. The asymptotic convergence of the magnetic moments is due to energy dissipation, without which a time-varying total magnetic moment would be present even for zero external magnetic field. Therefore, the existence of multiple metastable states is a necessary condition for hysteresis, but it is not sufficient.

The nature of the quasi-static changes in the input must be clarified to precisely define hysteresis. This clarification is done through the concept of a

rate-independent operator. Consider the thermostat relay, or *relay*, illustrated in Figure 2. Let $\alpha, \beta \in \mathbb{R}$ with $\beta \leq \alpha$. Suppose that $v(t)$ is continuous on the interval $[0, T]$, and let $u(0) = \zeta$, where $\zeta \in \{-1, +1\}$. For $t \in (0, T]$, define

$$A_t = \{\tau \in (0, t) : v(\tau) = \alpha \text{ or } \beta\},$$

and let

$$u(t) = \begin{cases} -1 & \text{if } v(t) \leq \beta, \\ 1 & \text{if } v(t) \geq \alpha, \\ u(t^*) & \text{if } \beta < v(t) < \alpha, \end{cases} \tag{1}$$

where

$$t^* = \begin{cases} \sup\{\tau : \tau \in A_t\} & \text{if } A_t \neq \emptyset, \\ 0 & \text{otherwise.} \end{cases} \tag{2}$$

The responses of this relay to sinusoidal inputs with frequencies 0.25 Hz and 25 Hz are shown in Figure 3(a). Note that plots of the output u versus the input v for the relay are identical for the two signals.

Next, consider the linear gear mechanism shown in Figure 4(a). This example illustrates the backlash phenomenon found in a typical gear mechanism. Although inertial effects are present in the operation of a gear mechanism, we ignore them here and focus on the kinematic relations to illustrate the hysteresis phenomenon. Equivalently, we capture the behavior of a gear mechanism operated in a quasi-static manner. We consider the lower gear to be the driven gear. Let $r = (r_0 - a)/2$ and $u(0) = \zeta$, where $\zeta \in \mathbb{R}$. For an input v that is monotone on the time interval $[0, T]$, the output is given by

$$u(t) = \max\{\min\{v(t) + r, \zeta\}, v(t) - r\}. \tag{3}$$

The gear mechanism in Figure 4(a) is commonly described as the *play* operator [4], and (b) illustrates the behavior of the play operator. The response of the play operator to sinusoidal inputs of frequencies 0.25 and 25 Hz are shown in Figure 3(b). The plots of the output u versus the input v for the play operator are identical for the two signals. The responses of the relay and the play operator can be contrasted with the responses of a single-input, single-output system with poles at -0.5, -1.5 and no zeros, and with zero initial conditions, for the sinusoidal signals shown in Figure 3(c). Note that the response of all three systems depends on the choice of an initial state.

We denote a system with memory by the operator equation

$$y = \mathcal{F}[v; x_0], \tag{4}$$

where y and v are continuous functions of time and x_0 denotes the initial state. The operator $\mathcal{F}$ is *rate independent* if it satisfies the following property. A continuous increasing function $\theta : [0, T] \to [0, T]$ satisfying $\theta(0) = 0$ and

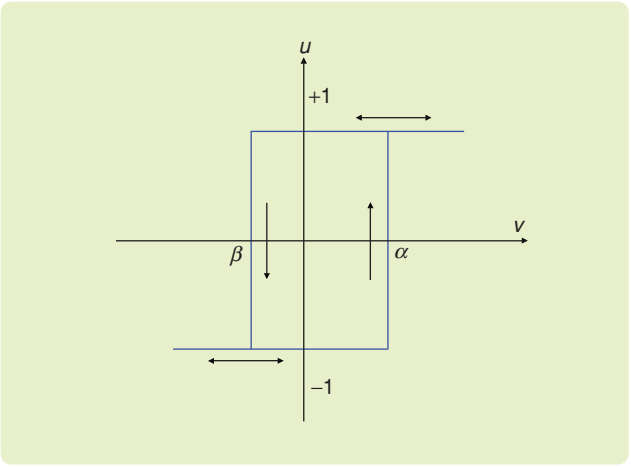

FIGURE 2 A thermostat relay characterized by a pair of thresholds (β, α). The output of the relay is $+1$ when the input is greater than α, -1 when the input is smaller than β, and remains unchanged while the input stays within $[\beta, \alpha]$.

$\theta(T) = T$ is an *admissible time transformation*. For a given piecewise-monotone input function v, suppose that $y(t) = \mathcal{F}[v; x_0](t)$. Then, $\mathcal{F}$ is rate independent if

$$y(\theta(t)) = \mathcal{F}[v; x_0](\theta(t)) = \mathcal{F}[v \circ \theta; x_0](t), \tag{5}$$

for all admissible time transformations θ. This definition of rate independence captures the idea that the output depends only on the values of the input and not on the rate at which the input achieves those values. The relay and the play operator satisfy this property as seen in Figure 3(a) and (b). In Figure 1, the input is changed in a quasi-static manner precisely so that the system has reached steady state when the measurements of H and B are recorded. Then the dependence of B on the history of H is only through the values achieved by H. This notion is mathematically captured by the concept of rate independence.

A *hysteresis operator* is a causal system with memory of the form (4) that is also rate independent [5]. A nonlinear dynamical system is a causal system with memory but is not generally rate independent. Both the relay and play operators satisfy the definition of a hysteresis operator. In addition, constitutive models for smart materials, such as the Prandtl-Ishlinskii (PI) and Preisach operators, are causal and rate independent, and thus are hysteresis operators. Note that the definition of a hysteresis operator implies that nonlinear dynamical systems and hysteresis operators are mutually exclusive. A different classification scheme can be found in [6], which separates a class of nonlinear systems called generalized Duhem models into those that are hysteretic and those that are not.

The definition of a hysteresis operator is general enough to encompass a variety of models. The input space for the operator is usually the space $C_{pm}[0, T]$ of continuous, piecewise-monotone functions. Extension to the space

of continuous functions $C[0, T]$ is typically obtained through the continuity of the operator on $C_{pm}[0, T]$. Specific forms of hysteresis operators are obtained by specifying the state space Ψ_0, the state evolution equation $\psi(t) = \Phi(v1_{[0,t]}, \psi_0)$, where $\Phi : C_{pm}[0, T] \times \Psi_0 \to \Psi_0$, and the output functional $Q : \Psi_0 \to \mathbb{R}$. Here $\psi_0 \in \Psi_0$, and $1_{[0,t]}$ is the function that is 1 on $[0, t]$ and 0 elsewhere. Thus a specific hysteresis operator takes the form

$$\mathcal{F}[v, \psi_0](t) = Q(\psi(t)). \tag{6}$$

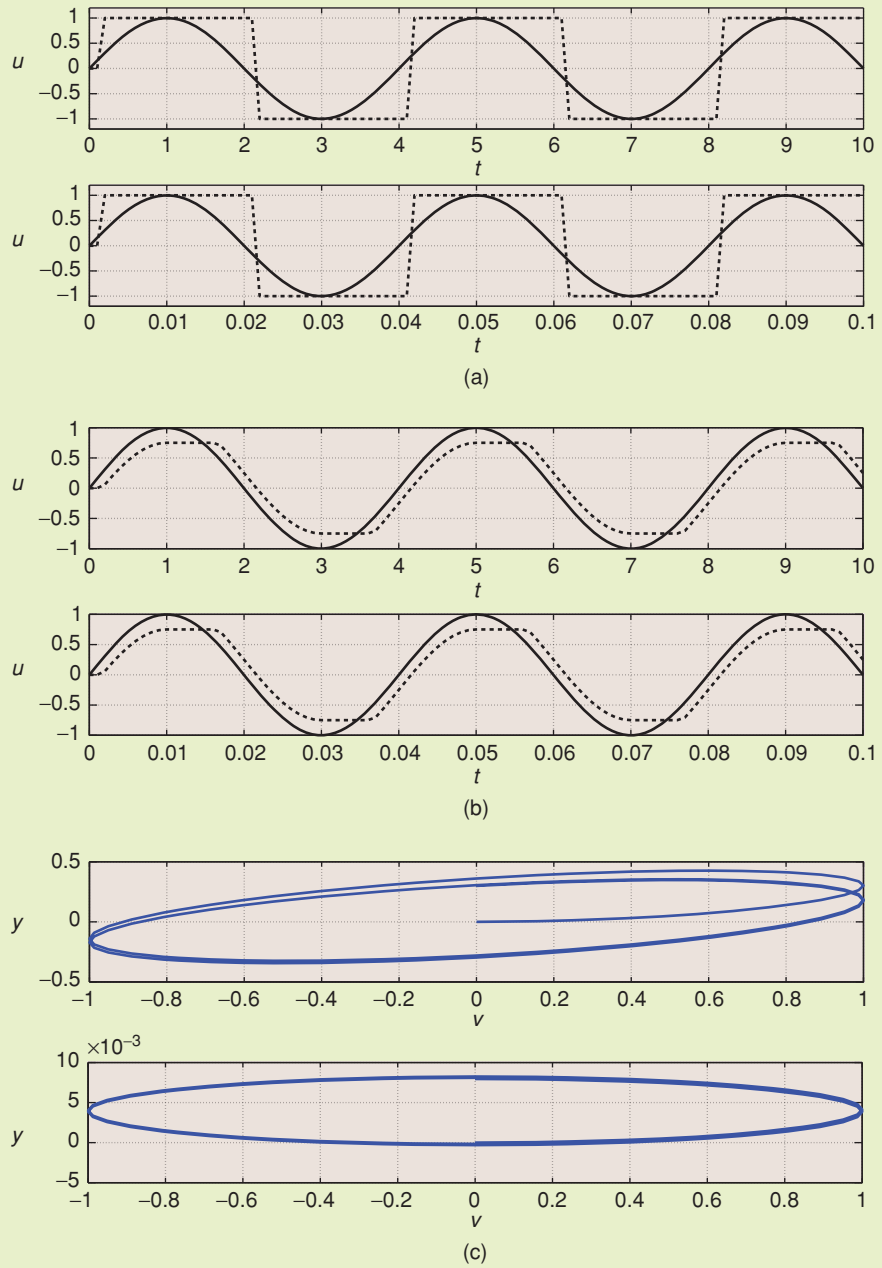

FIGURE 3 Two sinusoidal inputs of frequencies 0.25 Hz and 25 Hz are applied to (a) a relay, (b) a play operator, and (c) an asymptotically stable, second-order linear system. For each pair of plots in (a), (b), and (c), the upper plot shows the response to the 0.25-Hz input, while the lower plot shows the response to the 25-Hz input. Solid lines represent the input, and dashed lines represent the output. The units of the input and output are irrelevant. Note that the input and output signals for the relay and play operators are identical after time scaling as seen in (a) and (b). The input versus output graph for the linear system shown in (c) depends on the frequency of the input.

The dependence of $\psi(t)$ on $v1_{[0,t]}$ ensures that the current state depends only on past and current values of the input. Continuity properties of the operator $\mathcal{F}$ then depend on the continuity properties of Φ and Q on their respective domains. Mathematical properties of Φ and Q also determine whether $\mathcal{F}$ enjoys various properties such as the existence of major loops, minor-loop closure, energy dissipation, and monotonicity. All of these properties arise in the context of ferromagnetic hysteresis.

In engineering applications, hysteresis operators appear in conjunction with a system of differential equations. For example, consider a dc motor connected to a load through a gearbox. We define a *system with hysteresis* to be a series, parallel, or feedback connection of a hysteresis operator and a dynamical system. This article primarily concerns control of systems with hysteresis composed of a hysteresis operator in a series connection with a linear system as shown in Figure 5. Such systems are found in modeling actuators based on smart materials [7], such as piezoelectrics [8], [9], magnetostrictives [10], [11], shape memory alloys [12], [13], and electroactive polymers [14]. Magnetic suspension actuators can be modeled with a similar

series connection, where the hysteresis operator has two inputs and a single output [15].

The particular ordering of the hysteresis operator and linear system in Figure 5 is motivated by the electromechanical mechanisms of smart materials. For example, when a voltage is applied to a piezoelectric actuator, the applied electric field induces polarization, which in turn induces stress in the piezoelectric material through electromechanical coupling. The resulting stress then serves as the input to the mechanical system of the actuator, which can typically be represented as linear dynamics, to produce the force or displacement output. In this example, the field-polarization relationship is hysteretic [7], and the electrodynamics involved is much faster than the mechanical dynamics, making the field-polarization map appear rate independent. With the hysteresis operator preceding linear dynamics, inverse hysteresis compensation is implementable. We note that there are systems that can be represented as a dynamical system preceding a hysteresis operator; one example is a plant followed by a smart-material sensor. However, the discussion of these systems is beyond the scope of this article.

THE PREISACH HYSTERESIS OPERATOR

Using the relay and play operator as building blocks, we can build complex hysteresis operators that exhibit more subtle properties than the elementary operators. For example, although the minor loop closure property is not displayed by either the relay or the play operator for all continuous, piecewise-monotone inputs, a parallel combination of either play or relay operators may display this property. Several possibilities exist for this construction, leading to operators with different mathematical properties. Of these constructions, we discuss the *Preisach hysteresis operator*, which is widely used in the fields of magnetics and smart materials [16], [17]. Although the Preisach operator is used to model magnetic materials, it does not yield information about the internal structure of the materials themselves. In this sense, the Preisach operator is a phenomenological or black-box model. In this section, we study the relation of the Preisach operator to the relay and play operators.

Definition of the Preisach Operator

Consider the relay described by (1) and depicted in Figure 2. The relay is denoted by $R_{\beta,\alpha}$, where α and β are scalars. The output $u_{\beta,\alpha}(t)$ of $R_{\beta,\alpha}$ depends on the input $v(t)$ and the initial output $v_{\beta,\alpha}(0)$ as given by $u_{\beta,\alpha}(t) = R_{\beta,\alpha}[v, u_{\beta,\alpha}(0)](t)$. Consider a continuous, piecewise-monotone input function $v(t)$, $t \in [0, T]$, where $u_{\beta,\alpha}(0) \in \{+1, -1\}$. The Preisach operator is constructed as a weighted superposition of relays, also called *Preisach hysterons*. For an input function $v(\cdot)$, the output of the Preisach operator is given by [17]

$$u(t) = \iint_{\alpha \geq \beta} \mu(\beta, \alpha) R_{\beta,\alpha}[v, u_{\beta,\alpha}(0)](t)\, d\beta\, d\alpha, \qquad (7)$$

where $\mu : S \to \mathbb{R}$ is a nonnegative, integrable function on the half plane $S = \{(\beta, \alpha) : \alpha \geq \beta\}$. The set S is the Preisach plane (although it is a half plane), while μ is the Preisach density function. For every point (β, α) of S there exists a unique relay $R_{\beta,\alpha}$ and vice versa. We denote the action of the Preisach operator by the equation

$$u(t) = \Gamma[v, \phi_0](t), \quad t \in [0, T], \qquad (8)$$

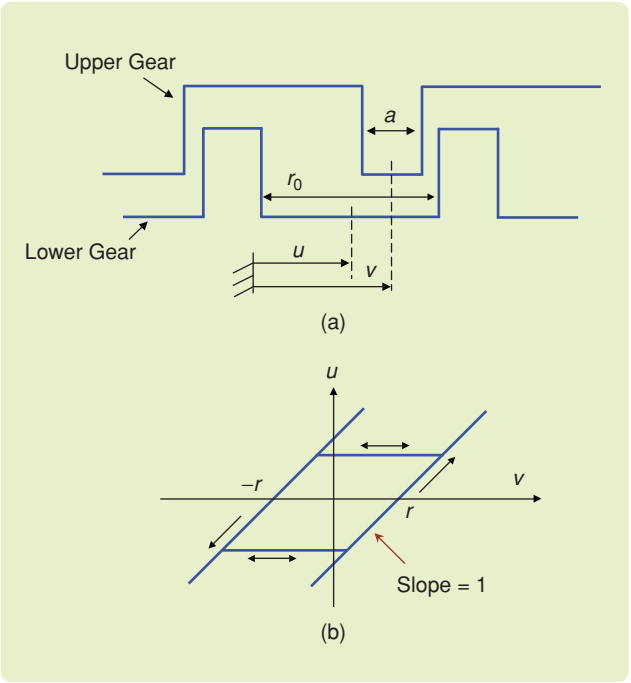

FIGURE 4 The backlash phenomenon in a gear mechanism. (a) Illustration of the gear mechanism. The upper gear drives the lower gear. The center v of the tooth in the upper gear represents the input, while the center u of the slot corresponding to the upper tooth represents the output. (b) The play operator. The play operator captures the kinematic input-output behavior of the gear mechanism, where the characterizing parameter r represents the difference between the slot width r_0 and the tooth width a.

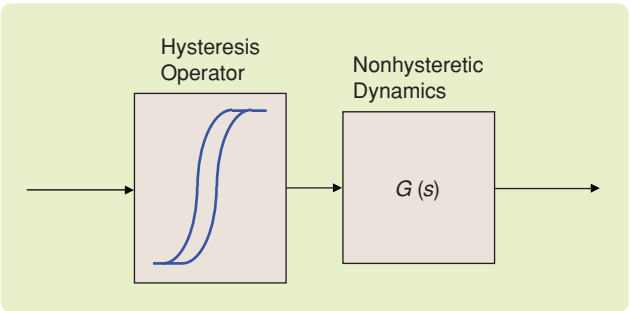

FIGURE 5 A system with hysteresis that captures the behavior of smart material-actuated systems. This system consists of the series connection of a hysteresis operator and a linear system G, with the hysteresis appearing at the input of the linear system. When the hysteresis operator precedes the linear dynamics (as shown), inverse hysteresis compensation is implementable.

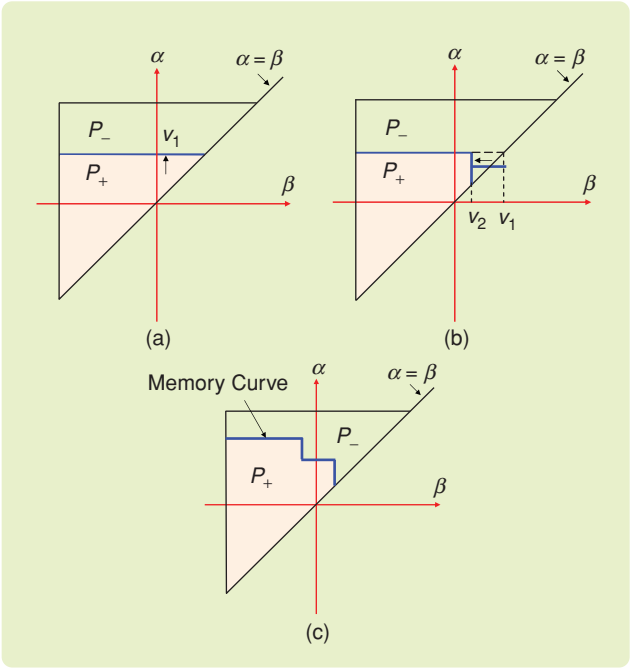

FIGURE 6 Memory curve structure for the Preisach operator. P_+ and P_- represent the regions on the Preisach plane where the corresponding hysteron outputs are positive and negative, respectively. (a) When the input monotonically increases, hysterons whose $\alpha-$thresholds are less than the current input are switched to $+1$, creating an upward-moving horizontal line as part of the boundary separating P_+ and P_-. (b) When the input monotonically decreases, hysterons whose $\beta-$thresholds are greater than the current input are switched to -1, creating a vertical segment moving to the left as part of the boundary between P_+ and P_-. (c) An arbitrary, piecewise-monotone input creates a memory curve that has a staircase structure. The corners of the memory curve remember the dominant maximal and minimal values of the input in the past, while the intersection of the memory curve with the line $\alpha = \beta$ gives the current input value.

where ϕ_0 represents the initial state of the operator, with $\phi_0(\beta, \alpha) = u_{\beta,\alpha}(0)$. Thus the initial state for the Preisach operator is the set of initial conditions for each relay in S.

The time evolution of the state for the Preisach operator is best understood using the Preisach plane. For simplicity, let $P \subset S$ be a compact set, and suppose that μ vanishes outside P. At each time t, the domain P consists of the sets, $P_+(t)$ and $P_-(t)$, where $P_\pm(t) \triangleq \{(\beta, \alpha) \in P : u_{\beta,\alpha}(t) = \pm 1\}$.

Suppose that the input at time 0 is such that all of the hysterons in the domain P have output -1. Next, suppose that the input is increased monotonically to a value v_1 at time t. Then all of the relays $\mathcal{R}_{\beta,\alpha}$ with $\alpha < v_1$ have output $+1$, while those with $\alpha \geq v_1$ have output -1, as illustrated in Figure 6(a). If the input is then monotonically decreased from v_1 to v_2, all of the relays $\mathcal{R}_{\beta,\alpha}$ with $\beta > v_2$ along with those with $\alpha > v_1$ have output -1, as shown in Figure 6(b). Note that the status of the relays at the boundary of the two regions P_- and P_+ in Figure 6 does not influence the output due to the assumption on the density function μ in (7). For a piecewise-monotone input, the same procedure can be followed, and staircase-like curves that separate the region P_- from the region P_+ can be obtained, as illustrated in Figure 6(c). Thus the state of the Preisach operator at each instant is governed by a single curve in the (β, α) plane. This curve is a *Preisach memory curve*. The state space is the collection of Preisach memory curves, and, unlike the case of a linear system, it is not a vector space. The analysis of the memory curve reveals a connection between the Preisach operator and the play operator. For more details, see "Memory Structure of the Preisach Operator." Figure 6 shows that the intersection of the Preisach memory curve and the line $\alpha = \beta$ at each time t yields the current input value $v(t)$.

Characterization of the Preisach Operator

The output of the Preisach operator at time t can be rewritten as

$$u(t) = \iint_{P+} \mu(\beta, \alpha)\, d\beta\, d\alpha - \iint_{P-} \mu(\beta, \alpha)\, d\beta\, d\alpha, \qquad (9)$$

which is used to prove three fundamental properties of the Preisach operator, rate independence, minor loop

Memory Structure of the Preisach Operator

The state of the Preisach operator at each instant of time is given by a curve in the Preisach plane. Each curve encodes the set of past local maxima and minima of the input, with earlier smaller local maxima (or minima) replaced by later larger ones [4], [17]. This peculiar dependence of the current output on the past input is called *nonlocal memory* in [17]. Further insight into the memory structure can be gained by making a coordinate change. By denoting $r = (\alpha - \beta)/2$ and $s = (\alpha + \beta)/2$, the memory curve can be described as a function $s = \phi(r)$. A staircase memory curve in (β, α) coordinates translates to a curve with segments of slope ± 1 in (r, s) coordinates. Therefore, the set $\mathcal{M}_0$ of Preisach memory curves is defined as follows [4]. Let $R_{\text{supp}}(\phi)$ denote the largest value of r such that $\phi(r) \neq 0$, and define the set

$$\mathcal{M}_0 \triangleq \{\phi \mid \phi : \mathbb{R}_+ \to \mathbb{R}, |\phi(r) - \phi(\bar{r})| \leq |r - \bar{r}|, \quad \text{for all} \quad r, \bar{r} \geq 0, \ R_{\text{supp}}(\phi) < +\infty\}.$$

It can be shown that, for a piecewise-monotone function $v(t)$, $t \in [0, T]$, and an initial memory curve in $\mathcal{M}_0$, the memory curve $\phi_v(t)$ at each time $t \in [0, T]$ also belongs in $\mathcal{M}_0$ [4]. The proof of this fact uses an interesting relation between the play operator and Preisach operator. If we denote the memory curve by $s = \phi(r, t)$, which indicates the dependence of s on both r and the time t, then it turns out that, for each r, the dependence of s on t is given by the play operator.

closure, and congruence [17]. Equation (9) is also used to prove the characterization theorem for Preisach operators, which states that for every hysteresis operator with these properties, there exists a Preisach operator with the same input-output map as that of the hysteresis operator [4], [17]. In other words, these properties are necessary and sufficient for a hysteresis operator to be represented by a Preisach operator.

Rate Independence

Equation (9) shows that the output at each instant depends on the regions P_+ and P_-. These regions are completely determined by the Preisach memory curve that separates them. It can be seen from Figure 6 and shown analytically [4] that the memory curve is uniquely defined by the sequence of local maxima and minima of the input signal on the interval $[0, t]$ and the initial memory curve ϕ_0. Since the output depends only on the levels of the past input, the Preisach operator possesses the rate independence property.

Minor Loop Closure

If the input is increased from a value v_1 to $v_2 > v_1$ over a time interval $[t_1, t_2]$ and then subsequently decreased back to v_1 over the time interval $[t_2, t_3]$, the output satisfies $u(t_3) = u(t_1)$ because the memory curves at t_1 and t_3 are identical.

Congruence

Suppose that two different memory curves ψ_1 and ψ_2 intersect the line $\alpha = \beta$ at a common point, corresponding to the current input v_1, as illustrated in Figure 7(a). For either ψ_1 or ψ_2, first increase the input v monotonically from v_1 to v_2, then decrease v monotonically back to v_1, and finally increase it monotonically to v_2 again. For both cases, the region in the Preisach plane that is affected when v is decreased from v_2 to v_1 is the same triangle shown in the shaded area in Figure 7(b). Consequently, the corresponding change in the output is identical in both cases. A similar argument shows that, when the input v is increased back from v_1 to v_2, the change in output is again identical in both cases. Figure 7(c) illustrates these properties in the input-output graph, where i-a, i-b, i-c represent the input-output graph corresponding to the three phases of monotonic input change, starting with the memory curve i, where $i = 1, 2$. The segments 1-b and 1-c can be viewed as vertical translations of 2-b and 2-c, respectively, which is the congruence property. Figure 7(c) also illustrates the minor-loop closure property, where segments 1-b and 1-c, or 2-b and 2-c, form a closed loop.

Preisach-Like Operators

By hysteron, we mean a basic building element for a hysteresis operator. The relay is also known as the *Preisach hysteron*. Taking variants of the Preisach hysteron as building blocks, we can obtain *Preisach-like* operators using weighted superposition of these new hysterons. For example, using the play operator, shown in Figure 4(b), or the stop operator, shown in Figure 8(a), as hysterons, we obtain the PI operators of play or stop type, respectively. Note that both play and stop operators are parameterized by a single variable r. Another example is the Preisach-Krasnosel'skii-Pokrovskii (PKP) operator, which is built on PKP hysterons. As illustrated in Figure 8(b), a PKP hysteron

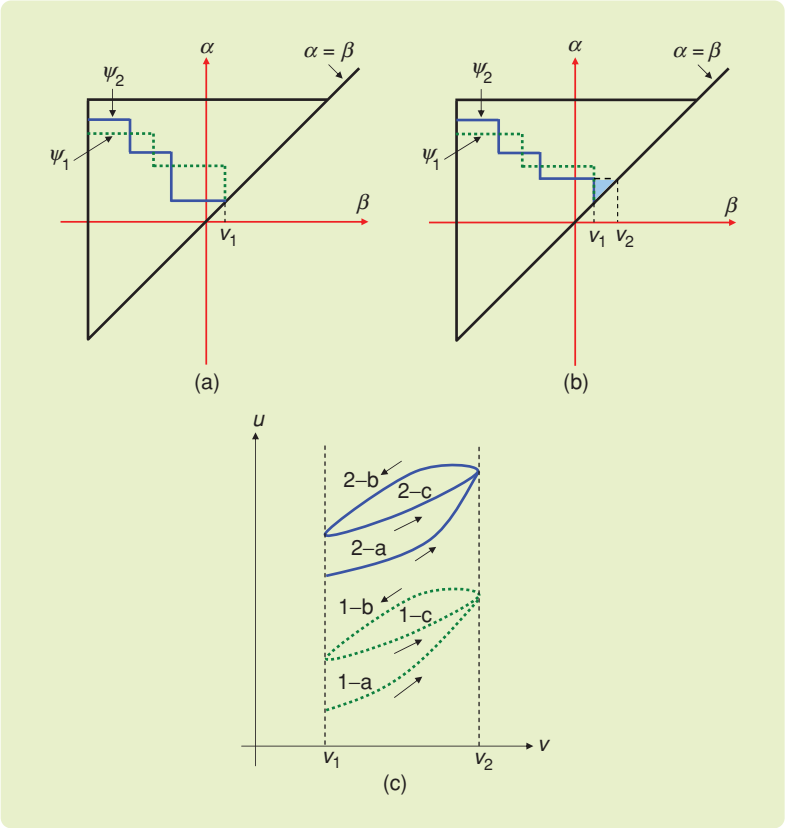

FIGURE 7 Illustration of the congruence property of the Preisach operator. In (a), two memory curves ψ_1 and ψ_2 intersect the diagonal line $\alpha = \beta$ at a common point, corresponding to the input value v_1. In (b), new memory curves are created after the input is increased from v_1 to v_2 and then decreased from v_2 to v_1. The changes in the operator output, corresponding to ψ_1 and ψ_2, respectively, are identical when v is decreased from v_2 to v_1 since the region affected by the input change is the same shaded, triangular area in (b). In (c), congruency is viewed in the input-output graph. Segments 1-a, 1-b, and 1-c represent the input-output responses during the three phases of input change, starting with the memory curve ψ_1, while, similarly, 2-a, 2-b, and 2-c represent the input-output responses starting with the memory curve ψ_2. Segments 1-b and 1-c can be viewed as vertical translations of 2-b and 2-c, respectively, explaining the term *congruence*. The minor loop closure property is also illustrated in (c).

can be thought of as a continuous version of the Preisach hysteron and is parameterized by (β, α). The parameter a, which is usually fixed for all hysterons in a PKP operator, modulates the slope of the ridges of the hysteron. The characteristic of a PKP hysteron is the same as that of a play operator, when it is unsaturated, namely, when its output is within the interval $(-1, 1)$.

Interestingly, the memory structure of the PKP operator when studied using the method in [17] turns out to be similar to that of the Preisach operator, and, in particular, the PKP operator satisfies rate independence, minor loop closure, and congruence. The latter fact implies that there is an equivalent Preisach operator with the same input-output characteristic as the PKP operator. The use of such an operator to model shape memory alloy actuators can be found in [12].

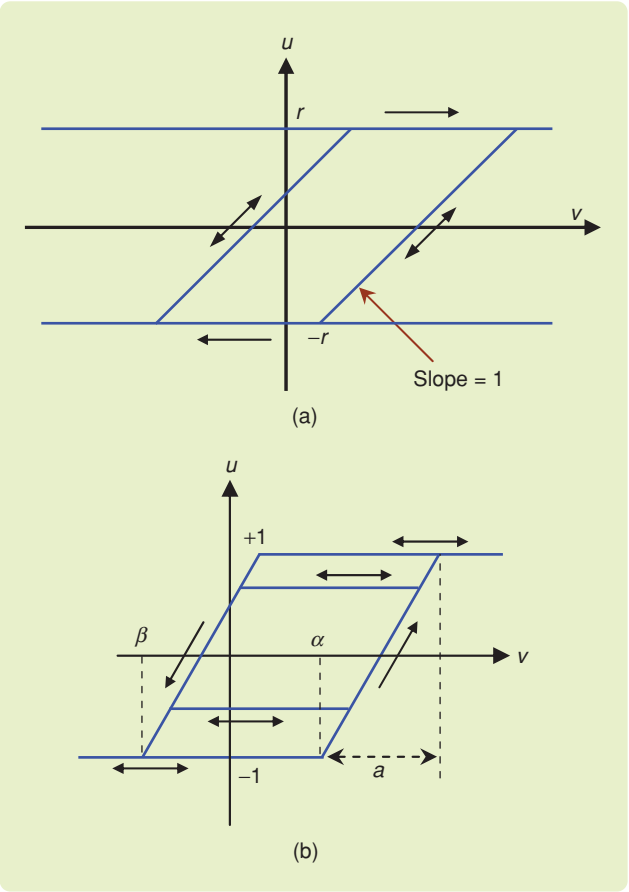

FIGURE 8 Variants of Preisach hysterons for the construction of Preisach-like operators. The stop operator in (a) is the dual of the play operator shown in Figure 4(b). Like the play operator, the stop operator is parameterized by a single variable r. Weighted superposition of play or stop operators leads to the Prandtl-Ishlinskii (PI) operators of play or stop type, respectively. (b) The Preisach-Krasnosel'skii-Pokrovskii (PKP) hysteron. A PKP hysteron, which is parameterized by a pair of variables (β, α), represents a continuous version of the relay. The weighted superposition of PKP hysterons leads to the PKP operator.

INVERSION OF PREISACH OPERATORS

Models of the type depicted in Figure 5 are useful for modeling the input-output characteristic of smart material actuators such as piezoelectrics, magnetostrictives, and shape memory alloys. The hysteresis operator shown in Figure 5 could be a Preisach operator [8], [11], [13], [14], or not [18], [19]. In this article, we consider the case in which the hysteresis operator is a Preisach operator Γ. Experiments show that feedback control without explicitly accommodating hysteresis performs poorly in tracking applications [11]. Hence, inclusion of hysteresis in the model is needed while designing controllers for systems with hysteresis.

A generic approach to controlling hysteretic systems is to combine inverse compensation with feedback [19], as illustrated in Figure 9. First, an approximate right inverse for the known hysteresis nonlinearity is constructed to cancel the hysteresis effect, and then a feedback controller $C(s)$ is designed to handle the linear system $G(s)$ and the inversion error.

Inversion is studied for various hysteresis operators in [11] and [19]–[21]. We focus on the problem of constructing the right inverse for the Preisach operator. Given a desired output function $u_d(t)$, $t \in [0, T]$, and an initial memory curve ψ_0 for a Preisach operator Γ, the inverse operator $\hat{\Gamma}^{-1}$, shown in Figure 10, generates $v(t)$ as the input to Γ, such that $u(t) = \Gamma[v, \psi_0](t) \approx u_d(t)$. In the

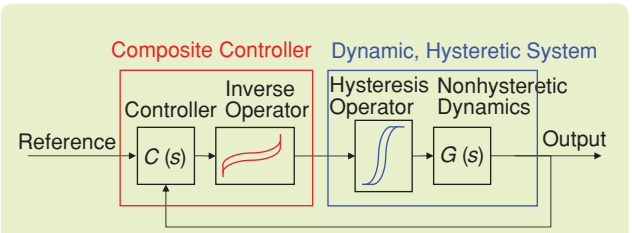

FIGURE 9 A generic approach to controlling a system with hysteresis. First, an inverse operator is constructed to approximately cancel the hysteresis nonlinearity. The feedback controller $C(s)$ is then designed to handle the linear dynamics $G(s)$ and the inversion error.

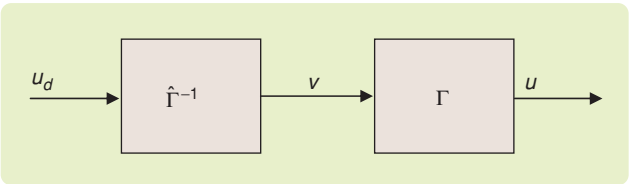

FIGURE 10 Illustration of hysteresis inversion. Here u_d represents the desired output for the Preisach operator Γ. The (approximate) inverse operator $\hat{\Gamma}^{-1}$ takes u_d as its input and outputs a signal v, such that the output of Γ under the input signal v is close to u_d. The evaluation of v depends on knowledge of the initial state (the memory curve at $t = 0$) of Γ. In practice, the memory curve at $t = 0$ is initialized as follows. Suppose that $[v_{\min}, v_{\max}]$ is the preselected range of values for the input. Before the start of the algorithm, either the input $v_{\min}$ or the input $v_{\max}$ is applied, which then sets the memory curve to be either $\beta = v_{\min}$ or $\alpha = v_{\max}$, respectively.

controller scheme, the signal $u_d(t)$ is generated by the controller $C(s)$ as illustrated in Figure 9.

Existence and continuity of the inverse of a Preisach operator are studied in [4], [5] and [20]. From an engineering perspective, continuity of the inverse operator is desirable since a small change in the function u_d leads to a small change in the function v. The notion of small change is quantified by describing norms on the sets in which u_d and v belong. It is shown in [4] and [5] that, if the Preisach density function is greater than zero on a thin strip along the line $\alpha = \beta$, then the Preisach operator $\Gamma : C_I[0, T] \to C_J[0, T]$ is invertible with a continuous inverse. Here, I and J are intervals where the input and the output of Γ take values, respectively. The sets $C_I[0, T]$ and $C_J[0, T]$ denote the spaces of continuous functions taking values in intervals I and J, respectively. The amplitudes of the input and the output are restricted based on practical considerations in smart material actuators and other physical systems that demonstrate hysteresis. The condition on the Preisach density function for the inverse to exist implies that parameter-free identification methods are preferred over methods that assume a particular form for the Preisach density. For details on identification methodologies, see "Identification of the Preisach Density Function."

For a Preisach operator with nonzero density on an arbitrarily thin strip along the line $\alpha = \beta$, it can be shown that the operator is a one-to-one mapping from the space of Hölder continuous functions $C^{0,\lambda}[0, T]$ into $C^{0,\eta}[0, T]$, where $\lambda < \eta$ (see [20, thm 2.1, 2.2] and [22, p. 54]). Since $C^{0,\eta}[0, T]$ is a proper subset of $C^{0,\lambda}[0, T]$ and consists of functions that are more regular than $C^{0,\lambda}[0, T]$, the inverse Preisach operator cannot possess the same smoothing property. Hence, the inverse of a Preisach operator is not itself a Preisach operator, and we have to solve (8) numerically to compute the input signal v when given the desired output signal u.

One approach to computing the inverse is a table-lookup procedure [17]. A computation procedure based on linearization is given in [8], while algorithms exploiting the *piecewise monotonicity* of Preisach operators, that is, increasing input leading to increasing output and vice versa, are reported in [12] and [23]–[25]. These algorithms can be classified into two groups, namely, fixed-point iteration methods [23], [26], and bisection type methods [12], [25]. A fixed-point iterative inversion algorithm is discussed below.

Fixed-Point Iterative Inversion Algorithm

This algorithm for solving (8) consists of two steps. First, the given continuous function $u_d \in C_J[0, T]$ is approximated by a piecewise-monotone function u_d' with a standard partition $0 = T_0 < T_1 < \cdots < T_N = T$ for some N, such that u_d' is monotone on each subinterval $[T_i, T_{i+1}]$, $i = 0, \ldots, N-1$. Second, the equation

Identification of the Preisach Density Function

In the inversion-based controller design paradigm for systems with hysteresis, two sources of error exist. The first source is the theoretical fact that the inverse Preisach operator does not have an analytical form in general, but algorithms for approximate inversion can be developed using the knowledge of the Preisach density function [20]. The implication is that, generically, $u_d(t)$ is not equal to $u(t)$ in Figure 10, even if the Preisach density function is accurately known. The second source of error is uncertainty in the Preisach density function.

Identification of the Preisach density function can be accomplished using methods that are either nonparametric or parametric. In nonparametric methods, the Preisach plane is discretized, and the Preisach density function is approximated by a piecewise-constant function on the grid. In parametric methods, a form for the density function, such as factorized Lorentzian, Gauss-Gauss, or lognormal-Gauss, is assumed, and the unknown parameters in the density function are estimated. It is shown in [20] that a nonzero value for the density on an arbitrarily thin strip along the line $\alpha = \beta$ in the Preisach plane implies the existence of a continuous inverse operator. The density functions assumed in parametric methods are nonzero along the line $\alpha = \beta$, and thus the question of existence of a continuous inverse is preemptively decided in favor of existence. In addition, although parametric methods typically involve fewer parameters than nonparametric methods, they seem to produce worse matches with experimental data than nonparametric ones [36].

Two nonparametric methods are available for estimating the Preisach density, namely, first-order reversals [17] and constrained linear least squares [27]. The accuracy of the identified model in reproducing the input-output graph of a given system with hysteresis can be improved by choosing a finer grid on the Preisach plane. The number of unknown parameters is $N(N+1)/2$, where N is the number of levels for the input signal [27]. The method of first-order reversals requires at least $N(N+1)/2$ data points using a carefully chosen input signal to estimate the density function [17]. Because of this requirement, the method becomes computationally expensive, and careful experimentation is required for large values of N. The constrained linear least squares method identifies a density function that minimizes

$$J = \frac{1}{2}\int_0^T \left(u(t) - \iint_{\alpha \geq \beta} \mu(\beta, \alpha) R_{\beta,\alpha}[v, \phi_0(\beta, \alpha)](t) \right)^2 d\beta\, d\alpha, \tag{S1.1}$$

subject to the condition $\mu(\beta, \alpha) \geq 0$ with the output signal $u(t)$, input signal $v(t)$, and initial memory ϕ_0 given. Subspace identification methods [27] can be used to produce estimates of the density function with fewer data points than the number of unknown parameters.

$$u_d'(t) = \Gamma[v, \phi_0](t), \quad t \in [0, T], \tag{10}$$

is solved for v, where ϕ_0 is a known memory curve. In practice, the memory curve at $t = 0$ is initialized as follows. Suppose that $[v_{\min}, v_{\max}]$ is the preselected range of values for the input. Before the start of the inversion algorithm, either input $v_{\min}$ or $v_{\max}$ is applied, which then sets the memory curve to be either $\beta = v_{\min}$ or $\alpha = v_{\max}$, respectively. Note that, for systems represented in Figure 5, the initialization step is feasible since the hysteresis operator precedes the dynamics and its input is directly accessible. For other configurations, such as a hysteresis operator following the dynamics, the initialization step as described earlier may not work.

The inversion problem reduces to inverting monotone functions when we restrict attention to each subinterval $[T_i, T_{i+1}]$. We assume for simplicity that $u_d \in C_J[0, T]$ is monotone in the following discussion. The proof of convergence for the algorithm relies on the piecewise monotonicity and Lipschitz continuity properties defined below.

Definition 1

A Preisach operator Γ is piecewise monotone if, for all monotone functions $v \in C([0, T])$, where $T > 0$, and for all initial memory curves ψ_0

$$(\Gamma[v, \psi_0](T) - \Gamma[v, \psi_0](0))(v(T) - v(0)) \geq 0. \tag{11}$$

Definition 2

A Preisach operator Γ is Lipschitz continuous if, for all $v_1, v_2 \in C([0, T])$, where $T > 0$, and for all initial memory curves ψ_0, there exists $C_L > 0$ such that

$$\|\Gamma[v_1(\cdot), \psi_0] - \Gamma[v_2(\cdot), \psi_0]\|_\infty \leq C_L \|v_1 - v_2\|_\infty, \tag{12}$$

where $\|v\|_\infty = \max_{t \in [0,T]} v(t)$ for $v \in C[0, T]$.

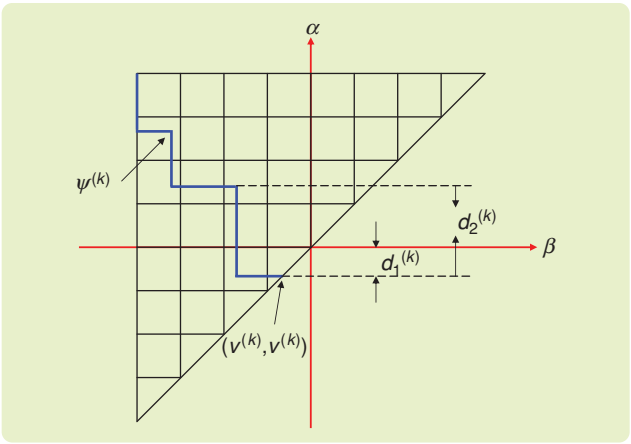

FIGURE 11 Illustration of the discretization grid on the Preisach plane and the parameters $d_1^{(k)}$ and $d_2^{(k)}$ involved in the inversion algorithm. The discretization level chosen here is $L = 8$. The distance d_1 represents the gap between the next input level on the discretization grid and the input value at the current iteration k, while d_2 represents the change of input required to erase the next corner of the memory curve. For an input change less than d_1 and d_2, the change in output is related to the change in input by a quadratic function.

It is shown in [4] that if μ is nonnegative then Γ is piecewise monotone, and if, in addition, μ is bounded on bounded subsets of the Preisach plane, then Γ is Lipschitz continuous as a mapping from $C_I[0, T]$ to $C_J[0, T]$. For a monotone function $u_d \in C_J[0, T]$ and an initial memory curve ψ_0, an approximate inverse function $v \in C_I[0, T]$ can be found by the iteration

$$v^{[0]} \equiv v_0, \tag{13}$$

$$v^{[k+1]} = v^{[k]} + \frac{u_d - \Gamma[v^{[k]}, \psi_0]}{C_L}, \quad k \in \mathbb{N}, \tag{14}$$

where the input value v_0 corresponds to the intersection of ψ_0 with the diagonal line on the Preisach plane. An induction argument shows that, for every k, $v^{[k]}$ is continuous and monotone [20]. Furthermore, it can be proved that $\Gamma[v^{[k]}, \psi_0] \to u_d$ uniformly on $[0, T]$ as $k \to \infty$ [20]. In other words, for every tolerance $\varepsilon > 0$, there exists a constant $N_\varepsilon > 0$ such that, for all $k \geq N_\varepsilon$,

$$\left\| \Gamma[v^{[k]}, \psi_0] - u_d \right\|_\infty \leq \varepsilon.$$

If the Preisach operator maps $C_I[0, T]$ to $C_J[0, T]$ with $I = [v_{\min}, v_{\max}]$, then N_ε can be taken to be the smallest integer greater than $C_L(v_{\max} - v_{\min})/\varepsilon$ as shown in [20].

Closest Match Algorithm for Preisach Operator with Piecewise Constant Density

For a piecewise-constant density function μ on the Preisach plane, the closest match algorithm, which uses the piecewise monotonicity property of the Preisach operator, is described in [24]. The name denotes the fact that the inversion of the Preisach operator depends on the estimated density function, which is a piecewise-constant approximation of the actual density function [27]. The closest match algorithm presented below is a modified version of the algorithm in [20] and [24]. We discretize the Preisach plane into a grid of square and triangular cells, with the triangular cells located along the diagonal; see Figure 11. The interval I on which the input takes its values is divided uniformly into L segments, where L is called the discretization level. Although the segments define a partition of the interval I, the input is not restricted to taking values only on the nodes of the partition. The density μ is assumed to be constant within each cell but can vary from cell to cell. The time interval $[0, T]$ is also discretized by a partition of the form $0 = T_0 < T_1 < \cdots < T_N = T$. The inversion problem is then reformulated as follows. Given the memory curve $\psi(n)$ at time T_n, find $v(n+1)$ such that the hysteresis output is equal (or close) to the desired value $u_d(n+1)$ for the next time instant, that is, $u_d(n+1) = \Gamma[v, \psi(n)](n+1)$.

We assume that the Preisach operator is piecewise monotone. Let the input and the output of the Preisach operator corresponding to $\psi(n)$ be $v(n)$ and $u(n)$, respectively, and suppose that $u_d(n+1) > u(n)$. The case $u_d(n+1) < u(n)$ can be treated analogously. The basic idea

behind the algorithm is that, when the change Δ_v of the input is sufficiently small, the change Δ_u of the output is related to Δ_v through the quadratic function

$$\Delta_u = a_2\Delta_v^2 + a_1\Delta_v, \tag{15}$$

where the coefficients a_1 and a_2 depend on the current memory curve. In this algorithm, the input is changed iteratively with each change being the smallest among three possibilities d_0, d_1, d_2. Here d_1 is the difference between the input value in the current iteration and the next node with a greater value in the input partition, d_2 is the smallest value of Δ_v that eliminates a corner of the memory curve, and d_0 is the solution Δ_v to (15) with Δ_u given by the difference between $u_d(n+1)$ and the output value in the current iteration. The closest match algorithm from [11], [28] is described next.

» **Step 1)** $v^{(0)} = v_0$, $u^{(0)} = u_0$, $\psi^{(0)} = \psi(n)$, $k = 0$;

» **Step 2)**

$$d^{(k)} = \min\left\{d_0^{(k)},\ d_1^{(k)},\ d_2^{(k)}\right\}, \tag{16}$$

$$v^{(k+1)} = v^{(k)} + d^{(k)}, \tag{17}$$

$$u^{(k+1)} = \Gamma[v^{(k+1)}, \psi^{(k)}], \tag{18}$$

where $\psi^{(k)}$ is the memory curve after $\{v^{(i)}\}_{i=1}^{k}$ is applied, and $d_0^{(k)}$, $d_1^{(k)}$, $d_2^{(k)}$ are determined in the following way (see Figure 11 for illustration):

- Let $d_1^{(k)} > 0$ be such that $v^{(k)} + d_1^{(k)}$ equals the next discrete input level.
- Let $d_2^{(k)} > 0$ be the minimum value such that applying $v^{(k)} + d_2^{(k)}$ eliminates the next corner of $\psi^{(k)}$.
- Compute $a_1^{(k)}, a_2^{(k)} \geq 0$ satisfying, for $0 < d < \min\{d_1^{(k)}, d_2^{(k)}\}$,

$$\Gamma[v^{(k)} + d, \psi^{(k)}] - \Gamma[v^{(k)}, \psi^{(k)}] = a_2^{(k)}d^2 + a_1^{(k)}d,$$

and let $d_0^{(k)} > 0$ be the solution to

$$u_d(n+1) - \Gamma[v^{(k)}, \psi^{(k)}] = a_2^{(k)}\left(d_0^{(k)}\right)^2 + a_1^{(k)}d_0^{(k)}.$$

If $d^{(k)} = d_0^{(k)}$, go to Step 3; otherwise let $k := k+1$ and go to Step 2.

» **Step 3)** $v(n+1) = v^{(k+1)}$ and stop.

Although the closest match algorithm is limited to piecewise-constant density functions, it is not as restrictive as it might seem at first glance. In particular, we can approximate an arbitrary square-integrable density function μ with a piecewise-constant density function in the L^2 norm as shown in [27].

ADAPTIVE INVERSE CONTROL

Open-loop inverse control requires precise knowledge of the hysteretic operator. When such knowledge is not available, feedback from the hysteresis output can be used to estimate the hysteresis parameters and ultimately reduce the inversion error. This *adaptive inverse control* approach is illustrated in Figure 12.

To explain the approach in more detail, we consider a Preisach operator Γ with a density function μ that is piecewise constant on a discretization lattice of level L. Figure 13 illustrates such a lattice for $L = 4$. Each cell in the lattice is numbered with the index going from 1 to $K = L(L+1)/2$. Denote by $\theta_{H,i}$ the density value of the cell i. Given a memory curve $\psi(n)$ at time instant n, each lattice cell i is separated into a region $C^+(n)$, where the corresponding hysterons have output $+1$, and a region $C^-(n)$, where the corresponding hysterons have output -1. Define the *signed area* of cell i at time n by $w_{H,i}$, which is defined by

$$w_{H,i}(n) = \text{ area of } C^+(n) - \text{ area of } C^-(n).$$

Suppose that the side of each cell has length of 1 in Figure 13. Given a memory curve as shown in Figure 13, the signed area of a shaded square cell is 1, that of a shaded triangular cell on the diagonal is 0.5, that of a clear square cell is -1, and that of a square cell with both shaded and

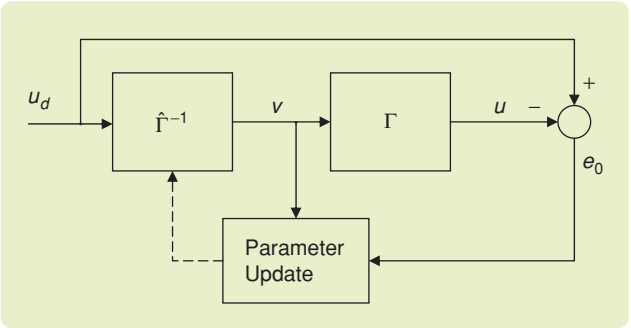

FIGURE 12 Schematic of adaptive inverse control. The inversion error $e_0 = u_d - u$ is used to update the hysteresis parameters online. It is assumed here that the output u of the hysteresis operator is available.

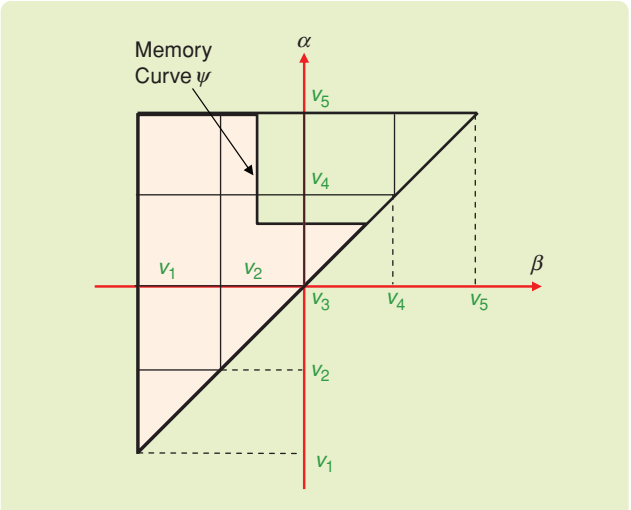

FIGURE 13 Illustration of the signed area of each lattice cell for a given memory curve. The signed area of a cell equals the area occupied by hysterons with output $+1$ minus the area occupied by hysterons with output -1. The signed areas of all cells are the components of the regressor vector for adapting hysteresis parameters.

clear regions takes value in $(-1, 1)$. The output $u(n)$ can be expressed as a linear combination of the unknown density values given by

$$u(n) = \sum_{i=1}^{K} \theta_{H,i} w_{H,i}(n) = \theta_H^T w_H(n), \tag{19}$$

where $\theta_H = (\theta_{H,1}, \ldots, \theta_{H,K})^T$ and $w_H = (w_{H,1}, \ldots, w_{H,K})^T$.

If the true values of θ_H are unknown, the inversion process has to be performed based on a parameter estimate $\hat{\theta}_H$. Equivalently, an operator $\hat{\Gamma}$ with parameter $\hat{\theta}_H$ is inverted, with its output

$$\hat{u}(n+1) = \hat{\Gamma}[v, \psi(n)](n+1) = \hat{\theta}_H^T w_H(n+1).$$

For the closest match inversion algorithm presented earlier, $\hat{u}(n+1) = u_d(n+1)$ if $|u_d(n+1)| \le \hat{u}_{sat}(n)$. Here $\hat{u}_{\text{sat}}(n)$ represents the saturation output value of $\hat{\Gamma}$ with parameter $\hat{\theta}_H(n)$. Since Γ and $\hat{\Gamma}$ have the common input $v(\cdot)$, they share $w_H(\cdot)$, and hence the prediction error is

$$e(n+1) = \hat{u}(n+1) - u(n+1) = \tilde{\theta}_H^T(n) w_H(n+1), \tag{20}$$

where $\tilde{\theta}_H \triangleq \hat{\theta}_H - \theta_H$.

The parameter $\hat{\theta}$ is updated using the gradient algorithm

$$\hat{\theta}_H(n+1) = \hat{\theta}_H(n) - \gamma \frac{e(n+1) w_H(n+1)}{w_H^T(n+1) w_H(n+1)}, \tag{21}$$

where the adaptation constant $\gamma \in (0, 2)$. If the true parameter θ_H is known to lie in a bounded set, a projection step can be used to ensure that the parameter estimate $\hat{\theta}_H$ also lies within this set.

The adaptive inverse control algorithm illustrated in Figure 12 is given by the following steps:

- **Step 1)** If $u_d(n+1) > \hat{u}_{\text{sat}}(n)$, $v(n+1) = v_{\max}$; if $u_d(n+1) < -\hat{u}_{\text{sat}}(n)$, $v(n+1) = v_{\min}$.
- **Step 2)** If $-\hat{u}_{\text{sat}}(n) \le u_d(n+1) \le \hat{u}_{\text{sat}}(n)$, perform the closest match inversion algorithm to find $v(n+1) = \hat{\Gamma}^{-1}[u_d(n+1), \psi(n)]$.
- **Step 3)** Update the hysteresis parameter to $\hat{\theta}_H(n+1)$ using (21).
- **Step 4)** Let $n := n+1$, and go back to Step 1.

It can be shown that the parameter estimate converges to some constant vector and the tracking error converges to zero for the adaptive inverse control algorithm [11]. Denoting $\delta(n) = \tilde{\theta}_H^T(n) \tilde{\theta}_H(n)$, we obtain from (20) and (21) that

$$\begin{aligned} \delta(n+1) &= \delta(n) - \left(1 - (\gamma - 1)^2\right) \frac{e^2(n+1)}{w_H^T(n+1) w_H(n+1)} \\ &\le \delta(n), \end{aligned} \tag{22}$$

since $(\gamma - 1)^2 < 1$ for $0 < \gamma < 2$. Since $\delta(n) \ge 0$, (22) implies that $\delta(n) \to \delta_\infty$ as $n \to \infty$, for some constant δ_∞. Consequently, $\hat{\theta}_H(n) \to \hat{\theta}_\infty$, for some constant vector $\hat{\theta}_\infty$. Furthermore, summing (22) over n leads to

$$\begin{aligned} \sum_{n=0}^{\infty} \frac{e^2(n+1)}{w_H^T(n+1) w_H(n+1)} &= \frac{1}{1 - (\gamma - 1)^2} (\delta(0) - \delta_\infty) \\ &< \infty. \end{aligned} \tag{23}$$

Since $0 < w_H^T(n+1) w_H(n+1) < C$ for some constant $C > 0$, (23) implies $e(n) \to 0$ as $n \to \infty$.

The tracking error $e_0(n+1) = u_d(n+1) - u(n+1)$ is different from the prediction error $e(n+1) = \hat{u}(n+1) - u(n+1)$. From the adaptation algorithm, the inversion at time $n+1$ is exact with $\hat{u}(n+1) = u_d(n+1)$ if $|u_d(n+1)| < \hat{u}_{\text{sat}}(n)$. If the latter condition fails, we can show $|e_0(n+1)| \le |e(n+1)|$. Indeed, suppose $u_{\text{sat}} \ge u_d(n+1) > \hat{u}_{\text{sat}}(n)$. The inversion algorithm produces $v(n+1) = v_{\max}$, resulting in $u_{n+1} = u_{\text{sat}}$ and $\hat{u}_{n+1} = \hat{u}_{\text{sat}}(n)$. Therefore, from $e(n) \to 0$, it follows that the tracking error $e_0(n) \to 0$ as $n \to \infty$.

Persistent Excitation Conditions

The conditions under which the limiting parameter estimate $\hat{\theta}_\infty$ equals the true parameter θ_H, in the adaptive inverse control of a Preisach operator, is of interest. The parameter convergence requires persistent excitation conditions on the regressor vector $w_H(\cdot)$, which can be further translated into conditions on the reference trajectory [29]. In contrast to persistent excitation conditions in the identification of linear systems, which are centered around the number of frequency components of the input signal [30], the conditions here involve the *reversal* behavior of the input [29].

Adaptive Inverse Control When Hysteresis Output Is Not Available

The adaptive inverse control algorithm in Figure 12 assumes the availability of the hysteresis output for feedback. In applications, the hysteresis module is coupled with other dynamics of a system, and its output cannot be measured. The scenario depicted in Figure 9 is typical, where the feedback signal is the output of the dynamics module. The algorithm discussed above can be extended to accommodate the latter requirement. Adaptive inverse control of a linear system preceded by a hysteresis operator, described by piecewise-linear characteristics, is studied in [19], where unknown parameters are present in both linear dynamics and hysteresis. Overparameterization is used to handle the bilinearly coupled parameters in hysteresis and dynamics in [19]. For systems involving Preisach operators, however, overparameterization is prohibitive because the number of parameters that are needed to characterize a Preisach operator is large, typically at the order of 10^2. To address the latter issue, an approach involving slow adaptation is explored in [31], where timescale separation is exploited for adaptation of hysteresis parameters and that of dynamics parameters.

RESULTS FROM EXPERIMENTS ON A MAGNETOSTRICTIVE ACTUATOR

The adaptive inverse control algorithm is tested on a magnetostrictive (Terfenol-D) actuator. Magnetostriction is the phenomenon of strong coupling between magnetic and mechanical properties in some ferromagnetic materials. An internal strain is developed in response to an applied magnetic field, and, conversely, an external mechanical force produces a change in magnetization distribution within the material. This phenomenon is used in both actuation and sensing applications. Figure 14(a) shows a schematic of a Terfenol-D actuator manufactured by Etrema Products, Inc., while Figure 14(b) shows the actuator used in the experiments. The magnetic field generated by the coil current controls the strain in the Terfenol-D rod, which translates into a displacement output of the actuator.

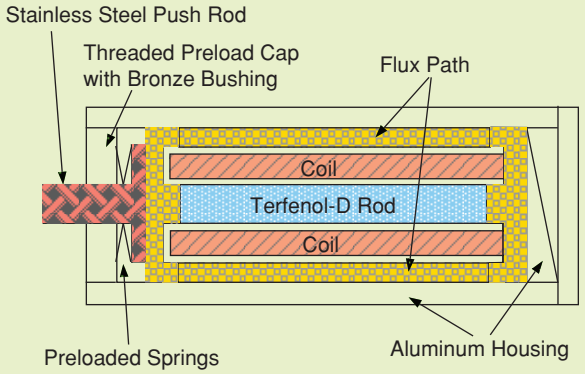

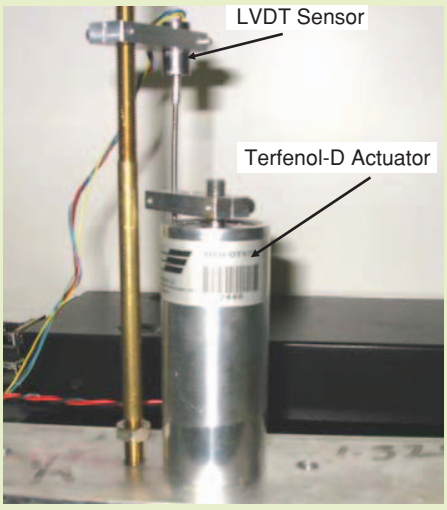

FIGURE 14 Terfenol-D actuator manufactured by Etrema Products, Inc. (a) Sectional view of the actuator design. The magnetic field generated by the coil current controls the strain in the Terfenol-D rod, which translates into a displacement output of the actuator. (b) Photo of the Terfenol-D actuator used in experiments. The tip displacement of the actuator is measured by a linear variable differential transformer (LVDT) sensor.

Figure 15 shows the actuation behavior of the actuator under various operating frequencies. The ferromagnetic hysteresis, coupled with the mechanical dynamics of the actuator and the dynamics of eddy current losses, results in rate-dependent loops between the displacement output and the current input [11], [18]. When operated in a low-frequency range (typically below 5 Hz), the displacement y can be related to the bulk magnetization M by a square law $y = a_1 M^2$ for some constant $a_1 > 0$, and the current input I can be related to the magnetic field H along the rod direction by $H = c_0 I$, where c_0 is the coil factor. Then the magnetostrictive hysteresis between y and I is fully captured by the ferromagnetic hysteresis between M and H, which is modeled by the Preisach operator.

Figure 16 shows the results of tracking experiments for a 1-Hz sinusoidal reference signal using the adaptive inverse control method with $\gamma = 0.5$ and 0.2, respectively. In the experiments, a discretization level $L = 10$ is adopted for the Preisach density function. The current input applied to the magnetostrictive actuator is also displayed in addition to the reference trajectory, the achieved trajectory, and the tracking error. It can be seen that when γ is 0.2, the trajectory converges to the steady state slower but with smaller tracking error due to lower sensitivity to the noise. Figure 17(a) shows the current input at steady state versus the desired trajectory, which is the graph of the inverse hysteresis operator $\hat{\Gamma}^{-1}$. Figure 17(b) shows the achieved trajectory versus the current input at steady state. Figure 17(c) shows the net effect of combining inverse compensation with the system with hysteresis, by plotting the achieved displacement versus the desired one at steady state (after 10 s). The largest error, which is in the region $[55, 60]$ μm, is about ± 0.5 μm.

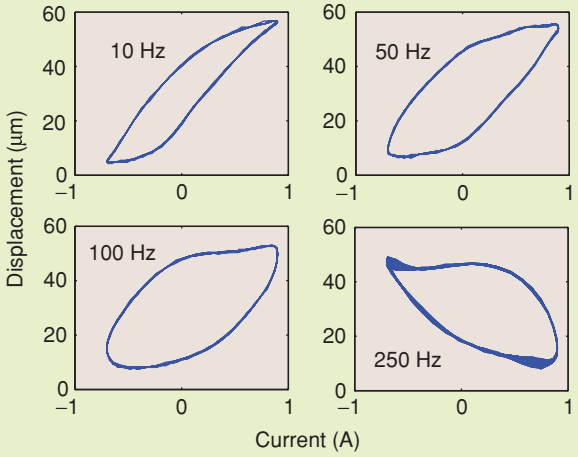

FIGURE 15 Behavior of a Terfenol-D actuator under various operating frequencies. Ferromagnetic hysteresis coupled with the mechanical dynamics of the actuator and the dynamics of eddy current losses results in frequency-dependent loops when the displacement output is plotted against the current input.

A PARALLEL PARADIGM FOR INVERTING PREISACH OPERATORS

Despite the capability of Preisach operators in modeling sophisticated hysteretic behaviors in physical systems, the complexity of their inverses presents a bottleneck in high-speed applications, such as control of piezoelectric actuator-based ultrafast nanopositioning for atomic force microscopy imaging. In particular, the efficient computation of the inverse of a Preisach operator using a general-purpose digital signal processor (DSP), which has to process a large number of hysterons sequentially, is challenging. To address this challenge, a parallel paradigm for the inversion of Preisach-like operators is presented in [32], which exploits the massive parallelism offered by field-programmable gate arrays (FPGAs).

An FPGA is a silicon device containing high-density programmable logic components and interconnects, which can be reconfigured by the end user (hence the term "field

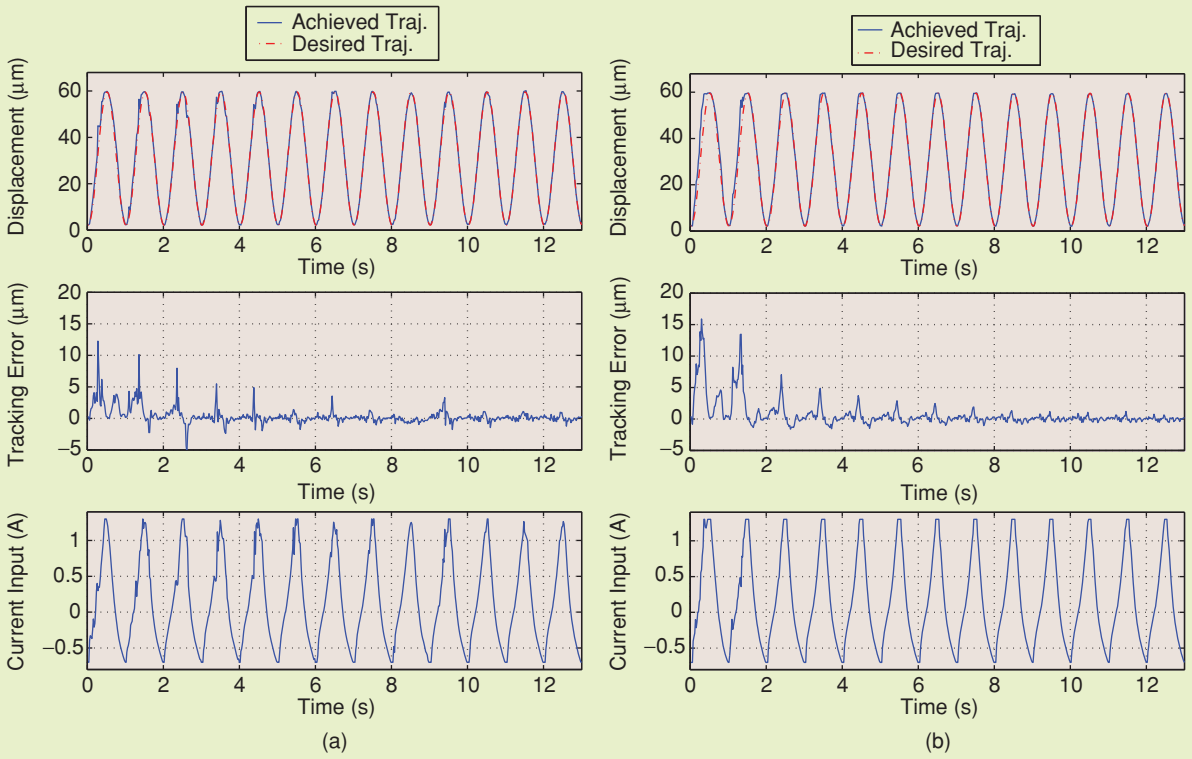

FIGURE 16 Experimental results for tracking a sinusoidal reference trajectory using adaptive inverse compensation. (a) Adaptation constant $\gamma = 0.5$ and (b) adaptation constant $\gamma = 0.2$. In both cases, the tracking error decreases after a few seconds of adaptation. With $\gamma = 0.2$, the convergence is slower than with $\gamma = 0.5$, but the steady-state error is also smaller. (Reproduced from [29].)

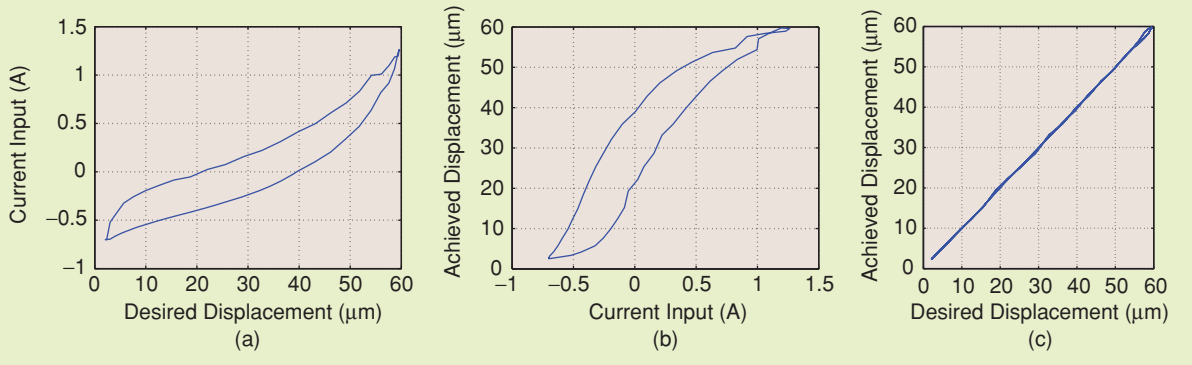

FIGURE 17 (a) Current input versus desired displacement at the steady state, (b) achieved displacement versus current input, and (c) achieved displacement versus desired displacement over the full operational range of the actuator after 10 s of adaptation (Reproduced from [29]). This figure illustrates the characteristics of the inverse compensator, shown in (a), those of the hysteretic plant, shown in (b), and the net effect of combining the inverse compensator and the hysteretic plant, shown in (c). The 45° line in (c) indicates that the hysteretic effect is cancelled.

programmable'') to perform fast application-specific processing [33]. The speed and processing power of FPGAs are comparable to those of application-specific integrated circuit (ASIC) chips, but they offer several advantages over ASICs, for example, instant manufacturing turnaround, low startup costs, and ease of design changes. The parallel paradigm of FPGAs is especially suitable for computing the inverses of Preisach-like operators. We know that the inversion process typically involves evaluating the output of a Preisach-like operator, and the operator is parallel in nature since all hysterons receive the same input. In addition, the characteristics of a hysteron can often be best described using logic elements, leading to convenient implementation of hysterons on FPGAs.

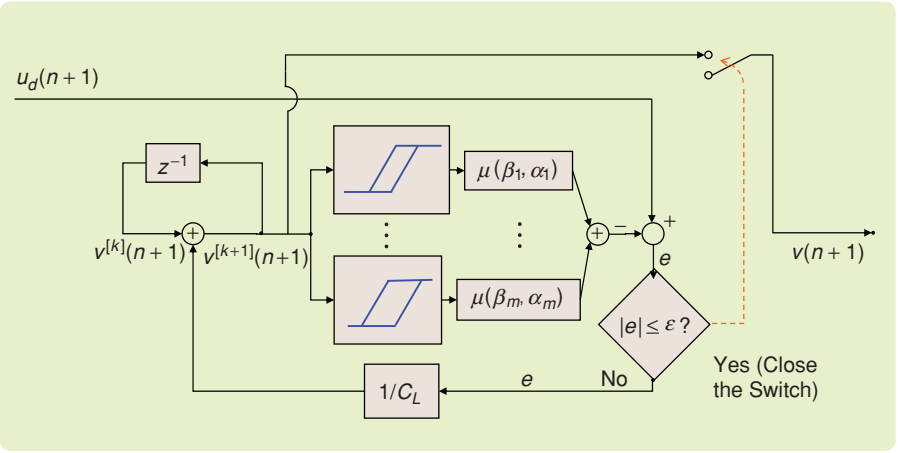

FIGURE 18 Schematic for implementing the iterative hysteresis inversion algorithm using a field-programmable gate array. Here n is the index of time instants, and k is the index of iteration for each time instant. Taking $u_d(n+1)$ as the input and $v(n+1)$ as the output, the system within the shaded region realizes the inverse compensator. When the inversion error is smaller than the given tolerance ε, the value $v^{[k+1]}(n+1)$ is taken as the inversion output.

A Unified Inversion Framework for Preisach-Like Operators

Suppose that a Preisach-like operator is piecewise monotone and Lipschitz continuous with Lipschitz constant C_L, where piecewise monotonicity and Lipschitz continuity are defined analogously as in definitions 1 and 2. We adopt a fixed-point iteration-type algorithm of the form (13) and (14), that is,

$$v^{[0]}(n+1) = v(n), \tag{24}$$

$$v^{[k+1]}(n+1) = v^{[k]}(n+1) + \frac{u_d(n+1) - \Gamma[v^{[k]}(n+1), \zeta(n)]}{C_L}, \tag{25}$$

where $\zeta(n)$ denotes the configurations of hysterons at time n. It is shown in [32] that, if $|u_d(n+1)| \le u_{\text{sat}}$, then $v^{[k]}(n+1)$ produced by the algorithm (24) and (25) satisfies $\lim_{k\to\infty} v^{[k]}(n+1) = v^*(n+1)$, with $\Gamma[v^*(n+1), \zeta(n)] = u_d(n+1)$. Furthermore, given any $\varepsilon > 0$, we can find an integer N_ε, such that $|\Gamma[v^{[k]}(n+1), \zeta(n)] - u_d(n+1)| \le \varepsilon$, for $k \ge N_\varepsilon$.

Note that the piecewise-monotonicity and Lipschitz-continuity conditions are satisfied under mild requirements on the weighting function for various Preisach-like operators, but a classical Preisach operator with a finite number of hysterons is not continuous and thus not Lipschitz continuous.

FPGA Implementation of the Inversion Algorithm

Figure 18 shows the implementation of the hysteresis inversion algorithm (25) on an FPGA for the PKP operator. Note that although the evaluations of all hysterons can be performed in parallel, the summation on weighted hysteron outputs is a bottleneck. To minimize the computation time, an adder tree is implemented for the summation. For example, suppose that the number of hysterons $m = 8$. The first level of the adder tree has four adders, each adding the contributions from a pair of hysterons. The second level has two adders, each adding the results of a pair of adders from the previous level. The third and last level has just one adder, adding the results of the adders from the second level. Therefore, three clock cycles are needed to complete the summation operation. In general, the adder tree for m hysterons takes $\log_2 m$ clock cycles. Since the summation is the speed-limiting factor in the FPGA-based hysteresis inversion, the computational time scales as $O(\log_2 m)$ with respect to the number of hysterons m. This complexity is in contrast to the $O(m)$ time-complexity required by a general-purpose DSP. The inversion process in FPGA can be further sped up by pipelining the summation process.

As an example, the inversion algorithm (25) is implemented on a Xilinx Virtex-II Pro FPGA. The implementation uses only logic resources and deliberately avoids using the two on-chip PowerPC cores and RAM resources, which might not be available for low-end FPGAs. The implementation for inverting a PKP operator with 21 hysterons takes about 30% of the logic resources on the Virtex-II Pro. The device usage can be further reduced through optimization of resource allocation. Each iteration (25) in the inversion takes 11 clock cycles to complete, which implies close to 5×10^6 iterations per second when a 50-MHz clock is used.

Experiments are conducted to verify the FPGA-based inversion algorithm. A collection of weights is assigned to the 21 PKP hysterons. The values of the weights are shown in Figure 19. An example of the hysteresis loop for this PKP operator is shown in Figure 20. The range of the input and the output of the FPGA is set to be $[-10, 10]$ V through A/D and D/A interfaces.

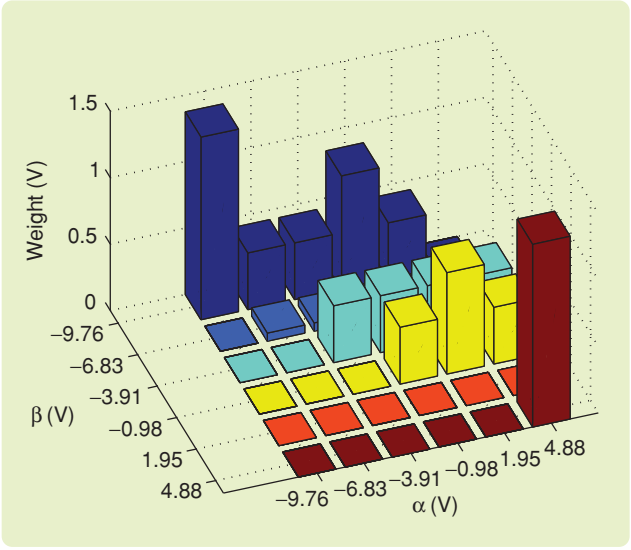

FIGURE 19 Distribution of Preisach-Krasnosel'skii-Pokrovskii (PKP) hysteron weights used in the simulation. The off-diagonal entries with nonzero weights result in the irreversible component of the overall PKP operator and hence the hysteresis effect.

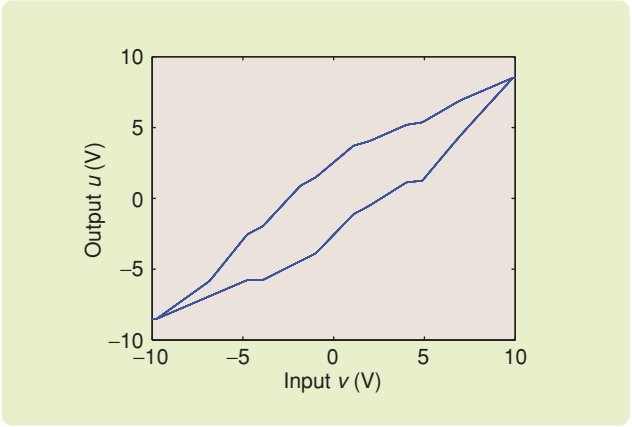

FIGURE 20 The output-input graph of the Preisach-Krasnosel'skii-Pokrovskii (PKP) operator with weights shown in Figure 19. This figure illustrates the hysteretic behavior of the PKP operator. The shape of the hysteresis loop is determined by the weights of individual PKP hysterons.

A reference trajectory $u_d(\cdot)$, generated from a dSpace DS1104 controller board, is sent to the FPGA hysteresis compensator. The inversion output $v(\cdot)$ is then converted to an analog signal and acquired by the dSpace board. The achieved output $u(\cdot)$ of the PKP operator is evaluated in Matlab based on the input $v(\cdot)$ and compared to the reference $u_d(\cdot)$. Figure 21(a) compares u_d and u when u_d is a sinusoidal signal with frequency 1000 Hz, while Figure 21(b) shows the result when u_d is a combination of 300 and 50-Hz signals. In both experiments, the tracking performance is satisfactory, where the tracking error is consistent with the set tolerance $\varepsilon = 0.1$ in the inversion.

These results show that the inversion of a Preisach operator can be implemented to track reference signals in the kilohertz range, which makes the inversion-based hysteresis control feasible for highly dynamic applications. Parallel adaptation of hysteresis parameters can be further implemented to realize embedded adaptive inverse control.

CONCLUSIONS

Inverse compensation is a fundamental technique in the control of systems with hysteresis. In this expository article, we present algorithms for constructing the inverse of the Preisach operator, a hysteresis model with application to magnetics, smart materials, terrestrial hydrology [34], and economics [35]. Adaptive inverse control is discussed for cases where hysteresis parameters are not known precisely. To meet the demand of highly dynamic applications, an embedded inversion approach is presented that exploits the parallelism offered by FPGAs.

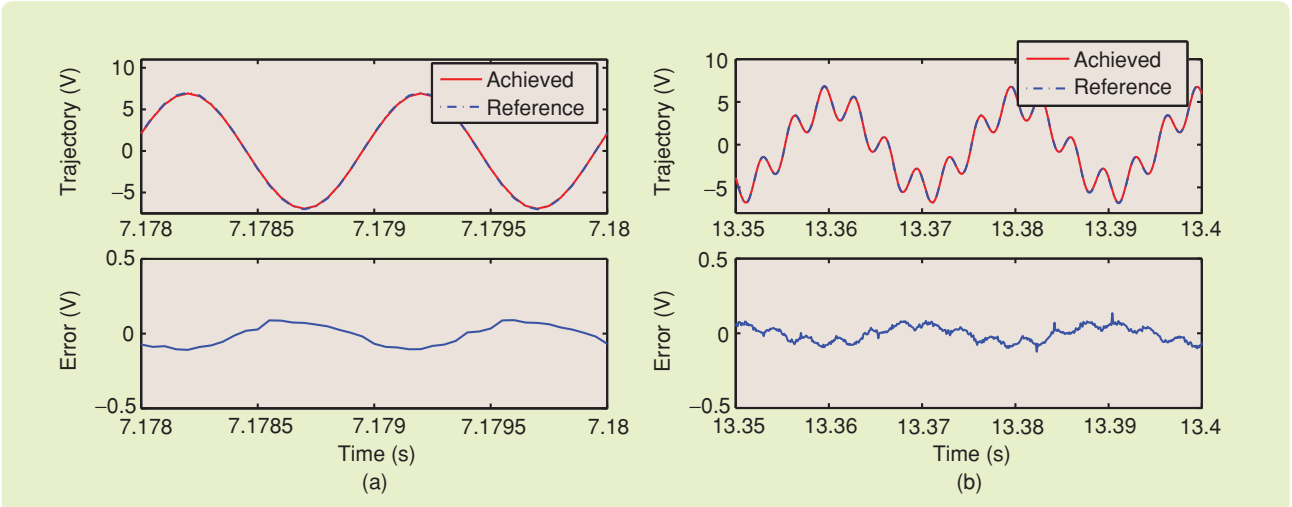

FIGURE 21 Embedded inversion-based tracking performance. (a) Results for a 1-kHz reference signal and (b) results for a reference signal consisting of 300- and 50-Hz components. In these experiments the inverse compensator is realized in a field-programmable gate array (FPGA), while the forward hysteresis operator is simulated by dSpace. In both (a) and (b), the tracking error is smaller than the set tolerance 0.1 V, which shows the potential of the FPGA-based inverse compensator in highly dynamic applications.

REFERENCES

[1] J.A. Ewing, *Magnetic Induction in Iron and Other Metals* (1, 2, and 3, Salisbury Court, Fleet Street). London, E.C.: The Electrician Printing and Publishing Co., Ltd., 1894.

[2] L.D. Landau and E. Lifshitz, "On the theory of the dispersion of magnetic permeability in ferromagnetic bodies," *Phys. Z. Soviet Un.*, vol. 8, pp. 153–169, 1935.

[3] W.F. Brown Jr., *Micromagnetics* (Interscience Tracts on Physics and Astronomy). New York: Wiley, 1963.

[4] M. Brokate and J. Sprekels, *Hysteresis and Phase Transitions*. New York: Springer-Verlag, 1996.

[5] A. Visintin, *Differential Models of Hysteresis*. New York: Springer-Verlag, 1994.

[6] J. Oh and D.S. Bernstein, "Semilinear Duhem model for rate-independent and rate dependent hysteresis," *IEEE Trans. Automat. Contr.*, vol. 50, no. 5, pp. 631–645, 2005.

[7] R. Smith, *Smart Material Systems: Model Development*. Philadelphia, PA: SIAM, 2005.

[8] W.S. Galinaitis and R.C. Rogers, "Control of a hysteretic actuator using inverse hysteresis compensation," in *Mathematics and Control in Smart Structures*, vol. 3323, V.V. Varadhan, Ed. Bellingham, WA: SPIE, 1998, pp. 267–277.

[9] D. Croft, G. Shed, and S. Devasia, "Creep, hysteresis, and vibration compensation for piezoactuators: Atomic force microscopy application," *J. Dyn. Syst., Meas., and Contr.*, vol. 123, no. 1, pp. 35–43, 2001.

[10] D. Davino, C. Natale, S. Pirozzi, and C. Visone, "Phenomenological dynamic model of a magnetostrictive actuator," *Physica B: Condensed Matter Physics*, vol. 343, pp. 112–116, 2004.

[11] X. Tan and J.S. Baras, "Modeling and control of hysteresis in magnetostrictive actuators," *Automatica*, vol. 40, no. 9, pp. 1469–1480, 2004.

[12] G. Webb, D. Lagoudas, and A. Kurdila, "Hysteresis modeling of SMA actuators for control applications," *J. Intell. Mat. Syst. and Struct.*, vol. 9, no. 6, pp. 432–448, 1998.

[13] S. Majima, K. Kodama, and T. Hasegawa, "Modeling of shape memory alloy actuator and tracking control system with the model," *IEEE Trans. Contr. Syst. Technol.*, vol. 9, no. 1, pp. 54–59, 2001.

[14] Z. Chen, X. Tan, and M. Shahinpoor, "Quasi-static positioning of ionic polymer-metal composite (IPMC) actuators," in *Proc. IEEE/ASME Int. Conf. on Advanced Intelligent Mechatronics*, Monterey, CA, 2005, pp. 60–65.

[15] S. Mittal and C.-H. Menq, "Hysteresis compensation in electromagnetic actuators through Preisach model inversion," *IEEE/ASME Trans. Mechatron.*, vol. 5, no. 4, pp. 394–409, 2000.

[16] F. Preisach, "Über die magnetische nachwirkung," *Zeitschrift für Physik*, vol. 94, pp. 277–302, 1935.

[17] I. Mayergoyz, *Mathematical Models of Hysteresis*. New York: Springer-Verlag, 1991.

[18] R. Venkataraman, "Modeling and adaptive control of magnetostrictive actuators," Ph.D. dissertation, Dept. Elec. Eng., Univ. Maryland, College Park, May 1999 [Onlne]. Available: http://www.lib.umd.edu/drum/bitstream/ 1903/6043/1/PhD_99-1.pdf.

[19] G. Tao and P. Kokotović, "Adaptive control of plants with unkown hystereses," *IEEE Trans. Automat. Contr.*, vol. 40, no. 2, pp. 200–212, 1995.

[20] R.V. Iyer, X. Tan, and P.S. Krishnaprasad, "Approximate inversion of hysteresis with application to control of smart actuators," *IEEE Trans. Automat. Contr.*, vol. 50, no. 6, pp. 798–810, June 2005.

[21] K. Kuhnen, "Modeling, identification and compensation of complex hysteretic nonlinearities: A modified Prandtl-Ishlinkskii approach," *Eur. J. Contr.*, vol. 9, pp. 407–418, 2003.

[22] M. Krasnoselskii and A. Pokrovskii, *Systems with Hysteresis*. New York: Springer-Verlag, 1989.

[23] R. Venkataraman and P.S. Krishnaprasad, "Approximate inversion of hysteresis: theory and numerical results," in *Proc. 39th IEEE Conf. Decision and Control*, 2000, pp. 4448–4454.

[24] X. Tan, R. Venkataraman, and P.S. Krishnaprasad, "Control of hysteresis: theory and experimental results," in *Modeling, Control and Signal Processing in Smart Structures*, vol. 4326, *Smart Structures and Materials*, V. Rao, Ed. Bellingham, WA: SPIE, 2001, pp. 101–112.

[25] G. Song, J. Zhao, X. Zhou, and J.A.D. Abreu-García, "Tracking control of a piezoceramic actuator with hysteresis compensation using inverse Preisach model," *IEEE/ASME Trans. Mechatron.*, vol. 10, no. 2, pp. 198–209, 2005.

[26] K.K. Leang and S. Devasia, "Iterative feedforward compensation of hysteresis in piezo positioners," in *Proc. 42nd IEEE Conf. Decision and Control*, Dec. 2003, pp. 2626–2631.

[27] R. Iyer and M. Shirley, "Hysteresis parameter identification with limited experimental data," *IEEE Trans. Magn.*, vol. 40, no. 5, pp. 3227–3239, 2004.

[28] X. Tan, "Control of smart actuators," Ph.D. dissertation, Elec. Eng. Dept., Univ. Maryland, College Park, MD, 2002 [Online]. Available: http://www. lib.umd.edu/drum/bitstream/1903/6344/1/PhD_2002-8.pdf.

[29] X. Tan and J.S. Baras, "Adaptive identification and control of hysteresis in smart materials," *IEEE Trans. Automat. Contr.*, vol. 50, no. 6, pp. 827–839, 2005.

[30] S. Sastry and M. Bodson, *Adaptive Control: Stability, Convergence, and Robustness*. Englewood Cliffs, NJ: Prentice-Hall, 1989.

[31] X. Tan and H.K. Khalil, "Control of unknown dynamic hysteretic systems using slow adaptation: Preliminary results," in *Proc. American Control Conf.*, New York, 2007, pp. 3294–3299.

[32] X. Tan and O. Bennani, "Fast inverse compensation of Preisach-type hysteresis operators using field-programmable gate arrays," in *Proc. American Control Conf.*, Seattle, WA, 2008, pp. 2365–2370.

[33] S. Brown and J. Rose, "FPGA and CPLD architectures: A tutorial," *IEEE Design and Test of Comput.*, vol. 13, no. 2, pp. 42–57, 1996.

[34] D. Flynn, H. McNamara, J.P. O'Kane, and A. Pokrovskii, "Application of the Preisach model to soil-moisture hysteresis," in *Science of Hysteresis*, G. Bertotti and I. Mayergoyz, Eds. Amsterdam: Academic, 2006, pp. 689–744.

[35] J. Darby, R. Cross, and L. Piscitelli, "Hysteresis and employment: A preliminary investigation," in *The Science of Hysteresis*, G. Bertotti and I. Mayergoyz, Eds. Amsterdam: Academic, 2006, pp. 667–699.

[36] O. Henze and W.M. Rucker, "Identification procedures of Preisach model," *IEEE. Trans. Magn.*, vol. 38, no. 2, pp. 833–836, 2002.

[37] J.A. Ewing, "On the production of transient electric currents in iron and steel conductors by twisting them when magnetized or by magnetising them when twisted," P*roc. Royal Soc. London.*, vol. 33, no. 2, pp. 21–23, 1881.

AUTHOR INFORMATION

Ram V. Iyer received the Ph.D. degree in electrical engineering from the University of Maryland, College Park in 1999. He is an associate professor in the Department of Mathematics and Statistics, Texas Tech University, Lubbock. He was a postdoctoral fellow during 1999–2000 at the University of Maryland, College Park, and a visiting scientist at the Control Center of Excellence, AFRL, Wright-Patterson, AFB, Ohio during 2000–2001. His interests include modeling, model identification, and control of smart materials and smart structures; numerical methods for control and observation of mechanical systems defined on Lie groups; and bio-inspired vision systems and their application to unmanned air vehicles. He was a NRC/AFOSR Summer Faculty Fellow for 2002–2004 and an ASEE/AFOSR Summer Faculty Fellow during 2005–2006. He is a Member of the IEEE, AIAA, and SPIE.

Xiaobo Tan (xbtan@egr.msu.edu) received the bachelor's and master's degrees in automatic control from Tsinghua University, Beijing, China, in 1995 and 1998, and the Ph.D. in electrical engineering from the University of Maryland at College Park, in 2002. From September 2002 to July 2004 he was a research associate with the Institute for Systems Research at the University of Maryland. In August 2004 he joined the Department of Electrical and Computer Engineering at Michigan State University as an assistant professor. His research interests include electroactive polymer sensors and actuators, modeling and control of smart materials, biomimetic robotics, bio/micro-manipulation, and collaborative control of unmanned vehicles. He is a recipient of the NSF CAREER award and an associate editor of *Automatica*. He can be contacted at the Department of Electrical and Computer Engineering, 2120 Engineering Building, Michigan State University, East Lansing, MI 48824, USA.